Chapter 13
New Effects in 1–3-Type Composites Based on Relaxor-Ferroelectrics Single Crystals

V.Yu. Topolov, C.R. Bowen and P. Bisegna

Abstract Two effects of the matrix subsystem on the piezoelectric performance and hydrostatic parameters are first studied in novel 1–0–3 composites that contain relaxor-ferroelectric single-crystal rods surrounded by a ferroelectric ceramic/polymer matrix with 0–3 connectivity. First, the influence of the mutual orientation of the poling direction of the single-crystal and ceramic components on the properties of the 1–0–3 composite is discussed to demonstrate advantages concerned with the high hydrostatic piezoelectric performance and large anisotropy of squared figures of merit. In a 1–0–3 $0.67Pb(Mg_{1/3}Nb_{2/3})O_3 - 0.33PbTiO_3$ single crystal/$(Pb_{1-x}Ca_x)TiO_3$ ceramic/araldite composite with $x = 0.20$–0.25, values of max $g_h^* \sim 10^2$ mV · m/N and $\max(d_h^* g_h^*) \sim 10^{-11}$ Pa^{-1} are achieved at specific volume-fraction and rotation-angle ranges due to the new orientation effect in the presence of a highly anisotropic 0–3 matrix. Second, the influence of the aspect ratio of ceramic inclusions on the piezoelectric and hydrostatic parameters of the 1–0–3 composite based on relaxor-ferroelectric SCs is studied. In this case, the elastic anisotropy of the 0–3 matrix plays the key role in forming the large effective parameters of the composite. The studied composites can be used in piezoelectric sensor, energy-harvesting and hydrophone applications.

V.Yu. Topolov (✉)
Department of Physics, Southern Federal University, Rostov-on-Don, Russia
e-mail: vutopolov@sfedu.ru

C.R. Bowen
Department of Mechanical Engineering, University of Bath, Bath, UK

P. Bisegna
Department of Civil Engineering and Computer Science, University of Rome 'Tor Vergata', Rome, Italy

I.A. Parinov et al. (eds.), *Advanced Materials*, Springer Proceedings in Physics 175, DOI 10.1007/978-3-319-26324-3_13

13.1 Introduction

Composites based on relaxor-ferroelectric single crystals (SCs) with high piezoelectric activity are an important group of advanced dielectric materials wherein the effective electromechanical properties and their anisotropy can be varied and tailored [1–4] in a wide range. Among the composite systems with a high piezoelectric activity and/or sensitivity [3–5], of particular interest are those based on domain-engineered relaxor-ferroelectric SCs such as $(1 - z)Pb(Mg_{1/3}Nb_{2/3})O_3 - zPbTiO_3$ (PMN–zPT) or $(1 - z)Pb(Zn_{1/3}Nb_{2/3})O_3 - zPbTiO_3$ (PZN–zPT) with compositions near the morphotropic phase boundary [6–9]. These composites are of interest due to the polarization orientation effect [4, 10–12] studied for a few connectivity patterns (e.g., 1–3, 2–2 and 0–3) in the last decade. This orientation effect depends not only on the connectivity of the composite system, but also on the electromechanical properties of the SC component, and this component can be poled along a specific crystallographic direction, for instance, along [001], [011] or [111] of the perovskite unit cell.

A potential method to increase the performance of the piezo-active composites is to modify their structure by introducing a third component [13–16]. Some modifications were studied for 1–3-type composites, and their parameters were compared to those of the conventional 1–3 ferroelectric ceramic (FC)/polymer composites. The presence of an anisotropic matrix in a 1–3-type composite structure opens up new and exciting possibilities of further tailoring the effective electromechanical properties of the composite and its hydrostatic parameters [14–16].

In this chapter, we show that the use of two ferroelectric components with distinct differences in their electromechanical properties leads to important effects that promote improving a few effective parameters of the three-component 1–3-type composite. Such a composite is of particular interest due to the complex inter-relationships in the fundamental triangle of ‘composition—structure—properties’ [17]. The aim of this chapter is to discuss advantages in effective parameters that are achieved by taking into account the new effects and the active role of the matrix subsystem in the 1–3-type SC/FC/polymer composites.

13.2 Orientation Effect in the 1–0–3 Composite with Two Polarization Directions

13.2.1 Model Concepts and Effective Parameters of the Composite

It is assumed that the composite consists of long SC rods embedded in a heterogeneous matrix (Fig. 13.1). The SC rods are in the form of the rectangular parallelepiped with a square base and square arrangement in the (X_1OX_2) plane. The main crystallographic axes X, Y and Z of each SC rod with the spontaneous

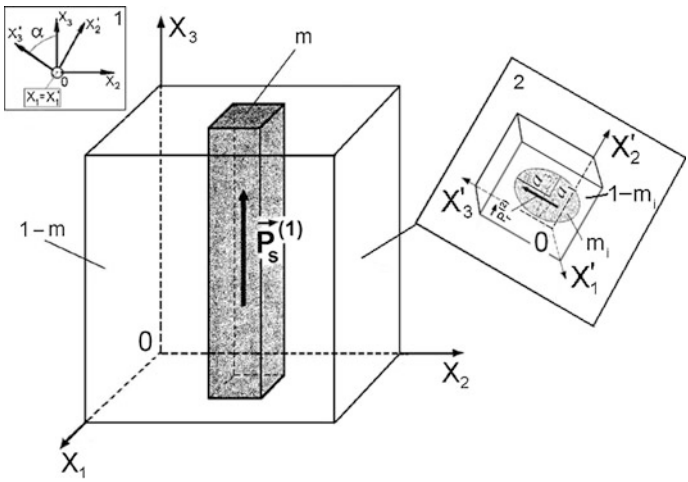

Fig. 13.1 Schematic of the 1–0–3 realxor-ferroelectric SC/FC/polymer composite. m and $1 - m$ are volume fractions of the SC and surrounding 0–3 matrix, respectively. Rotation of co-ordinate axes $(X_1'X_2'X_3') \rightarrow (X_1X_2X_3)$ is shown in *inset* 1, the 0–3 matrix is shown in *inset* 2. In the 0–3 matrix, m_i and $1 - m_i$ are volume fractions of the FC and polymer, respectively (reprinted from Topolov et al. [14], with permission from Elsevier)

polarization $\boldsymbol{P}_s^{(1)}$ are oriented as follows: X $\parallel OX_1$, Y $\parallel OX_2$ and Z $\parallel \boldsymbol{P}_s^{(1)} \parallel OX_3$. Spheroidal FC inclusions are surrounded by a large polymer matrix. The shape of each FC inclusion obeys the equation

$$(x_1'/a_1)^2 + (x_2'/a_2)^2 + (x_3'/a_3)^2 = 1 \tag{13.1}$$

relative to the axes of the rectangular co-ordinate system $(X_1'X_2'X_3')$ rotated by an angle α with respect to $(X_1X_2X_3)$ (inset 1 in Fig. 13.1). In (13.1), a_1, $a_2 = a_1$ and a_3 are semi-axes of the inclusion. To characterise its shape, we introduce the aspect ratio $\rho_i = a_1/a_3$. Centres of the inclusions occupy sites of a simple tetragonal lattice with unit-cell vectors parallel to the OX_k' axes. We assume that $0 < \rho_i < 1$, and the presence of prolate inclusions facilitates poling of the FC/polymer matrix due to a weaker depolarization effect. The remanent polarization vector of the FC inclusion is $\boldsymbol{P}_r^{(2)} \uparrow\uparrow OX_3'$, and OX_3' is the poling axis of the matrix (inset 2 in Fig. 13.1). The FC/polymer matrix represents a composite with 0–3 connectivity in terms of work [17, 18], and the three-component composite (Fig. 13.1) is described by 1–0–3 connectivity. Assuming that the linear sizes of each inclusion in the 0–3 matrix are much smaller than the length of the side of the square being intersected the rod in the (X_1OX_2) plane, we evaluate the effective properties of the 1–0–3 relaxor-ferroelectric SC/FC/polymer composite in two stages [14].

The first stage is related to the effective properties of the 0–3 composite matrix. Taking into account the electromechanical interaction between the piezo-active (poled FC) inclusions, the effective properties of the 0–3 composite matrix are

determined by either the effective field method (EFM) [4, 17] or finite element method (FEM) [17]. In the EFM, an electromechanical interaction in the FC/polymer matrix (see inset 2 in Fig. 13.1) is described using a local effective field. This effective field is determined by taking into account a system of interacting inclusions and boundary conditions based on inclusions with a spheroidal shape [4, 14, 15].

In terms of FEM modeling, COMSOL [19] is applied to obtain the volume-fraction dependence of the effective electromechanical properties of the 0–3 composite matrix. A representative unit cell, containing a spheroidal inclusion with a radius adjusted to yield the appropriate volume fraction m_i, is discretized using tetrahedral elements [4, 15]. The number of elements, depending on the aspect ratio ρ_i of the spheroidal inclusion, varies from 1,000,000 to 1,700,000. The unknown displacement and electric-potential fields are interpolated using linear Lagrangian shape functions. The corresponding number of degrees of freedom varies from 700,000 to 1,200,000. The following conditions are assumed at the inclusion—matrix interface: (i) perfect bonding (i.e., continuity of the displacement field) and (ii) continuity of the electric potential. Moreover, either Dirichlet or periodic boundary conditions are considered at the boundary of the parallelepiped representative unit cell 'inclusion—matrix' [14].

At the second stage, the effective electromechanical properties of the 1–0–3 composite are evaluated using the matrix method [4, 17]. The electromechanical properties of the SC rod and 0–3 composite matrix are averaged in the OX_1 and OX_2 directions, in which the periodic structure of the composite (Fig. 13.1) is observed, and take into account electromechanical interactions in a system of 'piezo-active rods—piezo-active matrix'. The effective electromechanical properties of the 1–0–3 composite in the co-ordinate system $(X_1X_2X_3)$ are given by

$$\| C^* \| = \| C^*(m,\, m_i,\, \rho_i, \alpha) \| = \begin{pmatrix} \| s^{*E} \| & \| d^* \|^t \\ \| d^* \| & \| \varepsilon^{*\sigma} \| \end{pmatrix}. \tag{13.2}$$

In (13.1), $\| s^{*E} \|$, $\| d^* \|$ and $\| \varepsilon^{*\sigma} \|$ are matrices of elastic compliances at electric field E = const, piezoelectric coefficients and dielectric permittivities at mechanical stress σ = const, respectively, and superscript 't' denotes transposition.

Based on the $\| C^* \|$ matrix from (13.1), we determine the following effective parameters of the 1–0–3 composite: piezoelectric coefficients g_{fl}^* from equation $\| d^* \| = \| \varepsilon^{*\sigma} \| \cdot \| g^* \|$, squared strain–voltage figures of merit

$$(Q_{33}^*)^2 = d_{33}^*\, g_{33}^*,\ (Q_{32}^*)^2 = d_{32}^*\, g_{32}^* \text{ and } (Q_{31}^*)^2 = d_{31}^*\, g_{31}^*, \tag{13.3}$$

hydrostatic piezoelectric coefficients

$$d_h^* = d_{33}^* + d_{32}^* + d_{31}^* \text{ and } g_h^* = g_{33}^* + g_{32}^* + g_{31}^*, \tag{13.4}$$

and squared hydrostatic figure of merit

$$(Q_h^*)^2 = d_h^* g_h^*. \tag{13.5}$$

It is assumed that electrodes applied to a composite sample (Fig. 13.1) are perpendicular to the OX_3 axis. The piezoelectric coefficients g_{fl}^* characterise the piezoelectric sensitivity of the composite. Squared figures of merit $(Q_{fl}^*)^2$ from (13.3) are used to characterise [4, 17] the piezoelectric sensor signal-to-noise ratio. The hydrostatic piezoelectric coefficients d_h^* and g_h^* from (13.4) describe [4, 17] the piezoelectric activity and sensitivity under hydrostatic loading of the composite sample for SONAR and hydrophone applications. The parameter $(Q_h^*)^2$ from (13.5) plays the role of the hydrostatic analog of $(Q_{3l}^*)^2$ from (13.3) and is used [17] to characterize the piezoelectric sensitivity under hydrostatic loading.

13.2.2 Components of the Composite

Among the components of the 1–0–3 composite, we mention [001]-poled domain-engineered PMN–0.33PT and PZN–0.08PT SCs with high piezoelectric activity, poled $(Pb_{1-x}Ca_x)TiO_3$ and modified $PbTiO_3$ FCs with a large piezoelectric anisotropy but moderate piezoelectric activity, and piezo-passive polymers such as araldite and polyurethane (Table 13.1). The hydrostatic piezoelectric coefficient $d_h^{(1)}$ evaluated in accordance with (13.4) exhibits different signs: $d_h^{(1)} > 0$ for the PMN–0.33PT SC, but $d_h^{(1)} < 0$ for the PZN–0.08PT SC. Hereafter, we use superscript '(1)' to denote the SC component and '(2)' to denote the FC component.

As follows from experimental data [7, 24], the coercive fields $E_c^{(n)}$ of the PMN–xPT SC ($n = 1$) and $(Pb_{1-x}Ca_x)TiO_3$ FC ($n = 2$) obey the condition $E_c^{(1)} \ll E_c^{(2)}$. Such a condition enables initial poling of the 0–3 matrix under a strong electric field with a subsequent poling of the SC rods in the composite (Fig. 13.1) under a lower electric field. We add that $(Pb_{1-x}Ca_x)TiO_3$ and related highly anisotropic FCs were used to form some 0–3 FC/polymer composites [17, 20, 25, 26].

13.2.3 Volume-Fraction and Orientation Dependence of Hydrostatic Parameters

As seen from Fig. 13.2, a and b, max g_h^* and max$[(Q_h^*)^2]$ of the PMN–0.33PT-based composite are achieved at a rotation angle $\alpha \approx 90°$ with a volume fraction of FC $m_i = 0.12$. Local max g_h^* relates to the volume fraction of SC $0.01 < m < 0.12$, however, the fabrication of a composite sample at $m < 0.03$ may be problematic in terms of the manufacturing tolerance [1, 2, 4, 17, 25]. The largest value of g_h^* at

Table 13.1 Elastic compliances s_{ab}^E (in 10^{-12} Pa^{-1}), piezoelectric coefficients d_{fl} (in pC/N) and relative dielectric permittivities $\varepsilon_{rr}^{\sigma}/\varepsilon_0$ of components at room temperature

Component	s_{11}^E	s_{12}^E	s_{13}^E	s_{33}^E	s_{44}^E	s_{66}^E	d_{31}	d_{33}	d_{15}	$\varepsilon_{11}^{\sigma}/\varepsilon_0$	$\varepsilon_{33}^{\sigma}/\varepsilon_0$
PMN–0.33PT SC, 4 mm symmetry [6]	69.0	–11.1	–55.7	119.6	14.5	15.2	–1330	2820	146	1600	8200
PZN–0.08PT SC, 4 mm symmetry [7]	87.0	–13.1	–70.0	141	15.8	15.4	–1455	2890	158	2900	7700
$(Pb_{0.80}Ca_{0.20})TiO_3$ FC [20]	6.04	–1.24	–1.25	6.21	14.7	14.6	–1.33	24.6	26.1	131	135
$(Pb_{0.75}Ca_{0.25})TiO_3$ FC [20]	6.00	–1.30	–1.30	6.18	14.8	14.6	–0.364	28.0	28.9	158	163
Modified $PbTiO_3$ FC [21]	7.50	–1.51	–1.10	8.00	17.9	18.0	–4.40	51.0	53.0	228	177
Araldite [22]	216	–78	–78	216	588	588	0	0	0	4.0	4.0
Polyurethane [23]	405	–151	–151	405	1110	1110	0	0	0	3.5	3.5

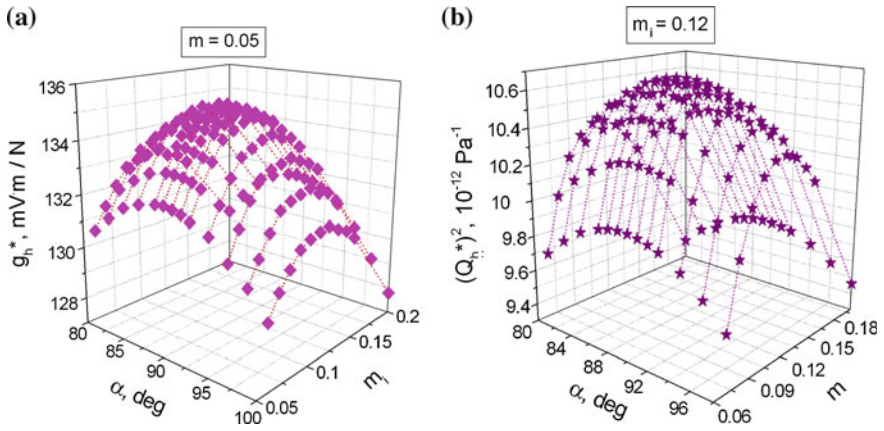

Fig. 13.2 Examples of the hydrostatic piezoelectric response of the 1–0–3 PMN–0.33PT SC/$(Pb_{0.75}Ca_{0.25})TiO_3$ FC/araldite composite at $\rho_i = 0.1$: **a** near local max $g_h^*(0.05, m_i, 0.1, \alpha)$, **b** near absolute max$\{[Q_h^*(m, 0.12, 0.1, \alpha)]^2\}$. Electromechanical properties of the 0–3 matrix at the first stage of averaging were determined by means of the EFM (reprinted from Topolov et al. [14], with permission from Elsevier)

$0.1 \le \rho_i \le 0.5$ relates to $m_i \approx 0.12$ and $0.01 < m < 0.03$, and in this m range, a local max g_h^* is observed at various values of m_i, ρ_i and α [14]. Our evaluations based on the EFM (0–3 matrix) and matrix method (1–3-type composite) lead to absolute max $d_h^* = 305$ pC/N at $m = 0.532$, $m_i = 0.12$, $\rho_i = 0.1$, and $\alpha = 90°$ [14].

Using the matrix method, we find for comparison, that the 1–3 PMN–0.33PT SC/araldite composite is characterized by absolute max $g_h^* = 158$ mV · m/N, absolute max$[(Q_h^*)^2] = 8.27 \cdot 10^{-12}$ Pa^{-1} and absolute max $d_h^* = 274$ pC/N at $m = 0.016$, 0.103 and 0.509, respectively [14]. At $m = 0.05$ for the 1–3 PMN–0.33PT SC/araldite composite, we obtain $g_h^* = 115$ mV·m/N, and this value is considerably smaller than g_h^* near the maximum point in Fig. 13.2a.

The large values of $(Q_h^*)^2$ (Fig. 13.2b) and d_h^* in the 1–0–3 composite are achieved due to the presence of a 0–3 matrix based on FC with piezoelectric coefficients $d_{3f}^{(2)}$ that obey the condition [20] $d_{33}^{(2)} / | d_{31}^{(2)} | \gg 1$. At $\alpha = 90°$, the remanent polarization vector $\boldsymbol{P}_r^{(2)}$ of each FC inclusion (see inset 2 in Fig. 13.1) is parallel to OX_2, and this $\boldsymbol{P}_r^{(2)}$ orientation leads to a decrease in $| d_{32}^* |$ with minor changes in d_{31}^* and d_{33}^* (or g_{31}^* and g_{33}^*, respectively) as a result of the weak lateral piezoelectric effect in the 0–3 matrix. As a consequence of the reduced $| d_{32}^* |$, we observe an increase in both d_h^* and g_h^*.

The elastic anisotropy of the 0–3 matrix with highly prolate inclusions is an additional factor in increasing the hydrostatic parameters from (13.4) and (13.5). Ratios of the elastic compliances in the 0–3 $(Pb_{0.75}Ca_{0.25})TiO_3$ FC/araldite composite matrix are represented as follows:

$s^E_{11,0-3}/s^E_{12,0-3} = -2.21$, $s^E_{11,0-3}/s^E_{13,0-3} = -6.52$ and $s^E_{11,0-3}/s^E_{33,0-3} = 1.95$ at $\rho_i = 0.1$ and $m_i = 0.10$, and

$s^E_{11,0-3}/s^E_{12,0-3} = -2.52$, $s^E_{11,0-3}/s^E_{13,0-3} = -3.51$ and $s^E_{11,0-3}/s^E_{33,0-3} = 1.25$ at $\rho_i = 0.3$ and $m_i = 0.10$.

This means that a significant decrease of $|\, s^E_{11,0-3}/s^E_{13,0-3} \,|$ and $|\, s^E_{11,0-3}/s^E_{33,0-3} \,|$ is observed with a weakening of the piezoelectric activity of the 0–3 composite.

The orientation effect considered in the 1–0–3 composite favours an increase in $(Q^*_h)^2$ and d^*_h near its maxima by approximately 29 % and 11 %, respectively, in comparison to a 'traditional' two-component 1–3 PMN–0.33PT SC/araldite composite [14]. The studied 1–0–3 composite is attractive due to large values of local maxima of d^*_h, g^*_h and $(Q^*_h)^2$ at m_i = const, especially at $m_i < 0.15$.

13.2.4 Anisotropy of Squared Figures of Merit

An important feature of the studied 1–0–3 composite consists in a large anisotropy of squared figures of merit from (13.3). For instance, the inequality

$$(Q^*_{33})^2/(Q^*_{3j})^2 \geq 10 \; (j = 1 \;\text{ and }\; 2) \tag{13.6}$$

holds at volume fractions of SC $m_{Q1} \leq m \leq m_{Q2}$ which depend on the rotation angle α (Fig. 13.3). The validity of condition (13.6) is achieved due to the 0–3 FC/polymer matrix with a significant elastic and piezoelectric anisotropy at $m_i = 0.50$ and $\rho_i = 0.1$. The presence of prolate FC inclusions has a significant influence on the electromechanical properties of the 0–3 matrix, and the anisotropy of these properties promotes the validity of condition (13.6) for the 1–0–3 composite. Values of $m_{Q2} < 0.1$ may be a result of the high piezoelectric activity of the SC while $d^{(1)}_{33}/d^{(2)}_{33} \approx 100$. We note that for the PMN–0.33PT SC, condition $(Q^{(1)}_{33})^2/(Q^{(1)}_{31})^2 = (Q^{(1)}_{33})^2/(Q^{(1)}_{32})^2 = (d^{(1)}_{33}/d^{(1)}_{31})^2 \approx 4.5$ holds (see Table 13.1).

13.2.5 Comparison of Effective Parameters

The effective parameters obtained using different methods are given for comparison in Table 13.2. To predict the effective properties of the 0–3 composite matrix at the first stage of calculations, we use either the EFM or one of two FEM models. Either Dirichlet (FEM-1) or periodic (FEM-2) boundary conditions are enforced on the boundary of the representative unit cell of the 0–3 FC/polymer matrix. At the second stage of calculations, we use the matrix method that is applicable to the 1–3 composite structure with planar interfaces [14]. The use of Dirichlet boundary conditions gives rise to a higher piezoelectric activity of the 0–3 matrix, whereas

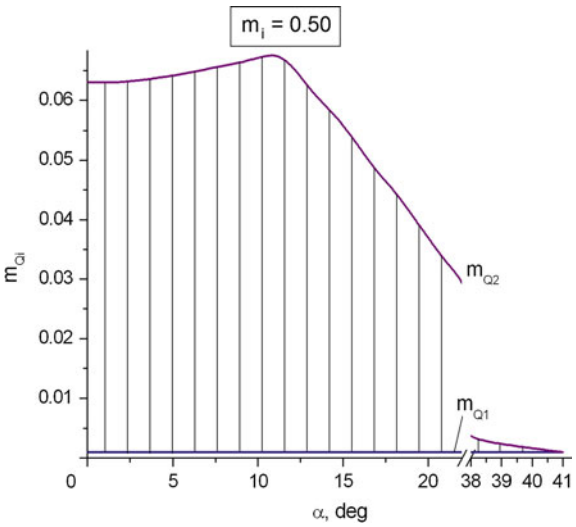

Fig. 13.3 Region of validity of condition (13.6) (hatched area) in the 1–0–3 PMN–0.33PT SC/$(Pb_{0.75}Ca_{0.25})TiO_3$ FC/araldite composite at $\rho_i = 0.1$ and $m_i = 0.50$. Electromechanical properties of the 0–3 matrix at the first stage of averaging were determined by means of the EFM (reprinted from Topolov et al. [14], with permission from Elsevier)

Table 13.2 Hydrostatic piezoelectric coefficient g_h^* (in mV · m/N) and squared hydrostatic figure of merit $(Q_h^*)^2$ (in 10^{-12} Pa^{-1}) of the 1–0–3 PMN–0.33PT SC/$(Pb_{0.80}Ca_{0.20})TiO_3$ FC/araldite composite at $\rho_i = 0.1$ and $\alpha = 90°$

Methods	g_h^* at $m_i = 0.10$, $m = 0.05$	g_h^* at $m_i = 0.10$, $m = 0.06$	g_h^* at $m_i = 0.10$, $m = 0.10$	g_h^* at $m_i = 0.15$, $m = 0.05$	g_h^* at $m_i = 0.15$, $m = 0.06$	g_h^* at $m_i = 0.15$, $m = 0.10$
EFM	133	121	86.6	133	122	89.1
FEM-1[a]	139	128	92.2	139	129	95.5
FEM-2[b]	128	117	84.3	127	118	86.5
Methods	$(Q_h^*)^2$ at $m_i = 0.10$, $m = 0.10$	$(Q_h^*)^2$ at $m_i = 0.10$, $m = 0.12$	$(Q_h^*)^2$ at $m_i = 0.10$, $m = 0.15$	$(Q_h^*)^2$ at $m_i = 0.15$, $m = 0.10$	$(Q_h^*)^2$ at $m_i = 0.15$, $m = 0.12$	$(Q_h^*)^2$ at $m_i = 0.15$, $m = 0.15$
EFM	10.2	10.3	10.0	10.3	10.4	10.2
FEM-1[a]	11.1	11.2	11.0	11.0	11.2	11.1
FEM-2[b]	9.53	9.59	9.40	9.32	9.46	9.36

Methods for prediction of properties of the 0–3 FC/polymer matrix are listed in the 1st column (reprinted from Topolov et al. [14], with permission from Elsevier)
[a]With Dirichlet boundary conditions, leading to higher piezoelectric activity of the 0–3 matrix
[b]With periodic boundary conditions, leading to lower piezoelectric activity of the 0–3 matrix

periodic boundary conditions lead to a lower piezoelectric activity than that obtained using the EFM method. The EFM results are close to average values obtained from the FEM models. Relatively small differences between the

parameters obtained using the EFM, FEM-1 and FEM-2 (Table 13.2) are accounted for by the very high piezoelectric activity of the SC rod in comparison to the 0–3 matrix.

We add for a further comparison, that in a 1–3 PZT FC/epoxy composite with aligned FC rods [27], values of max $d_h^* \approx 110$ pC/N and max$[(Q_h^*)^2] = 6.0 \cdot 10^{-12}$ Pa^{-1} are considerably lower than the maximum values of these parameters of the studied 1–0–3 composite (see, for instance, Fig. 13.2 and Table 13.2). According to data [17], a 1–3 PMN–0.33PT SC/araldite composite (a limiting case of the 1–0–3 composite at $m_i = 0$) is characterized by absolute max $d_h^* = 274$ pC/N (at $m = 0.509$), absolute max $g_h^* = 130$ mV · m/N (at $m = 0.016$) and absolute max $[(Q_h^*)^2] = 7.45 \cdot 10^{-12}$ Pa^{-1} (at $m = 0.115$). The aforementioned values are also smaller than those related to the 1–0–3 composite.

13.3 Aspect-Ratio Effect in the 1–0–3 Composite

13.3.1 Two Examples of the High Performance

In Sect. 13.3, we discuss the role of the aspect ratio ρ_i of FC inclusions in forming the large effective parameters of the 1–0–3 SC/FC/polymer composite. Hereafter, we consider the composite shown in Fig. 13.1 at $\alpha = 0°$ and vary ρ_i in the 0–3 FC/polymer composite matrix to show its influence on the effective parameters of the 1–0–3 composite.

Our recent results suggest that large changes in the piezoelectric coefficient g_{33}^* and squared figures of merit $(Q_{3j}^*)^2$ are observed (Fig. 13.4) at

$$0.01 < \rho_i < 2. \tag{13.7}$$

In the range (13.7), the shape of the FC inclusions changes from highly prolate ($\rho_i \ll 1$) to oblate ($\rho_i > 1$). Such changes in the microgeometry of the 0–3 composite matrix give rise to significant changes in its elastic properties and ratios of elastic compliances $s_{1b}^{(m),E}/s_{pq}^{(m),E}$ that then have a strong influence on the piezoelectric properties and their anisotropy in the 1–0–3 composite even at the small volume fraction of FC $m_i = 0.05$ (Fig. 13.4).

The correlation between the elastic compliance $s_{33}^{(m),E}$ of the 0–3 matrix and the squared figure of merit $(Q_{33}^*)^2$ of the composite was recently studied in work [15]. This correlation stems from the important role of $s_{33}^{(m),E}$ in the formation of the piezoelectric response of a 1–3 composite along the poling axis OX_3. In the case of the 1–0–3 composite (Fig. 13.1), the elastic anisotropy of its 0–3 matrix leads to a stronger link between $s_{33}^{(m),E}$ and $(Q_{33}^*)^2$, especially in the range (13.6).

Now we consider the hydrostatic piezoelectric coefficients of the 1–0–3 PZN–0.08PT SC/modified $PbTiO_3$/polyurethane composite (Fig. 13.5). Graphs in

Fig. 13.5 show the important role of the matrix subsystem in forming the hydrostatic response of the composite wherein the highly piezo-active SC component is characterized by $d_h^{(1)} = -20$ pC/N. Even at a relatively small volume fraction of the FC inclusions m_i, changes in the aspect ratio ρ_i give rise to considerable changes in the hydrostatic parameters, especially at $\rho_i > 1$. Moreover, max g_h^* (Fig. 13.5b) correlates with max d_h^* (Fig. 13.5a) because the relation [17] $g_h^* = d_h^*/\varepsilon_{33}^{*\sigma}$ is valid. In Fig. 13.5b we show a restricted range of volume fractions of SC m due to the significant decreasing g_h^* at $m > 0.2$ irrespective of the FC content. Changes in sgn d_h^* (Fig. 13.5a) take place at $m \approx 1$, when the SC rods play the dominating role in forming the piezoelectric properties of the composite. The use of the highly oblate FC inclusions ($\rho_i \gg 1$) leads to a lower dielectric permittivity of the 0–3 FC/polymer matrix at m_i = const and to a larger piezoelectric coefficient g_h^* of the composite at m = const (cf. curves 1 and 5 in Fig. 13.5b). We note that changes in the matrix elastic properties and their anisotropy become appreciable at aspect ratios $\rho_i > 1$.

13.3.2 Comparison of Data Obtained Using Different Methods

In Sect. 13.3.2, we consider a few effective parameters that were calculated for the 1–0–3 SC/FC/polymer composite by means of different methods. We also compare the effective parameters of the 1–0–3 composite to those known for related piezo-active composites.

First, for the PZN–0.08PT-based composite with oblate FC inclusions in the 0–3 matrix, we see good consistence between the hydrostatic piezoelectric coefficients calculated in two different ways (Table 13.3).

Second, we consider a specific case of a performance of a 1–0–3 SC/FC/polymer composite with a piezo-passive 0–3 matrix. It is assumed that the FC inclusions in the polymer matrix (Fig. 13.1) were not previously poled and, therefore, remain piezo-passive. By varying the aspect ratio ρ_i of these inclusions, we see changes in the effective parameters of the 1–0–3 composite (Table 13.4), however these parameters become larger than those in the case of the poled 0–3 matrix. This is a result of a decrease in the dielectric permittivity of the piezo-passive 0–3 matrix that leads to an appreciable decrease of the dielectric permittivity of the 1–0–3 composite $\varepsilon_{33}^{*\sigma}$ at relatively small SC volume fractions m. Results shown in Table 13.4 suggest that the elastic anisotropy in achieving high piezoelectric performance for the 1–0–3 composite remains a dominant factor irrespective of the piezoelectric activity of its 0–3 matrix. Thus, during the manufacture of samples of the 1–0–3 composite at $\alpha = 0°$ (Fig. 13.1), there is no need to pole the 0–3 FC/polymer matrix under a fairly strong electric field, as applied, for instance, to the $PbTiO_3$-type FC samples [24]. Changes in the volume fraction of FC, m_i, in the 0–3 matrix give rise to weaker changes in the effective parameters of the composite (Table 13.4) in

Table 13.3 Hydrostatic piezoelectric coefficients calculated for the 1–0–3 PZN–0.08PT SC/modified $PbTiO_3$ FC/polyurethane composite at $\rho_i = 100$

m_i	m	d_h^*, pC/N[a]	g_h^*, mV · m/N[a]	d_h^*, pC/N[b]	g_h^*, mV · m/N[b]
0.10	0.05	152	213	151	211
	0.10	266	146	262	145
	0.20	410	80.9	406	79.6
0.15	0.05	150	216	147	213
	0.10	260	151	254	148
	0.20	400	84.6	389	83.0
0.20	0.05	144	213	140	208
	0.10	250	151	241	147
	0.20	382	85.7	369	83.8
0.25	0.05	137	206	132	201
	0.10	237	148	227	144
	0.20	362	85.5	362	83.3

[a]Values were calculated using the EFM and matrix method at the first and second stages of averaging, respectively

[b]Values were calculated using the EFM and FEM at the first and second stages of averaging, respectively

Table 13.4 Effective parameters of the 1–0–3 PMN–0.33PT SC/modified $PbTiO_3$ FC/polyurethane composite in a case of a piezo-passive 0–3 matrix[a] (reprinted from Topolov et al. [15], with permission from Elsevier)

ρ_i	m_i	m	g_{33}^*, mV · m/N	$(Q_{33}^*)^2$, 10^{-12} Pa^{-1}	$(Q_{31}^*)^2$, 10^{-12} Pa^{-1}	d_h^*, pC/N	g_h^*, mV · m/N	$(Q_h^*)^2$, 10^{-12} Pa^{-1}
1.5	0.05	0.05	553	218	28.1	102	143	14.5
2.0	0.05	0.05	554	218	27.5	105	147	15.4
2.5	0.05	0.05	554	218	27.0	107	150	16.1
1.5	0.10	0.05	535	194	23.7	101	148	14.9
2.0	0.10	0.05	536	185	23.0	105	155	16.3
2.5	0.10	0.05	536	195	22.2	109	161	17.6
1.5	0.05	0.10	333	240	31.7	177	81.9	14.5
2.0	0.05	0.10	334	240	31.2	182	84.1	15.3
2.5	0.05	0.10	334	240	30.6	186	86.1	16.0
1.5	0.10	0.10	328	220	27.7	176	86.2	15.2
2.0	0.10	0.10	328	221	26.8	195	90.2	16.6
2.5	0.10	0.10	328	220	25.9	191	93.5	17.9

[a]Effective properties of the 0–3 FC/polymer matrix were evaluated by means of the EFM

comparison to changes caused by the volume fraction of SC, m. These weaker changes are concerned with the high piezoelectric activity of the SC rods and their parallel orientation along the poling axis: at such an arrangement, even minor

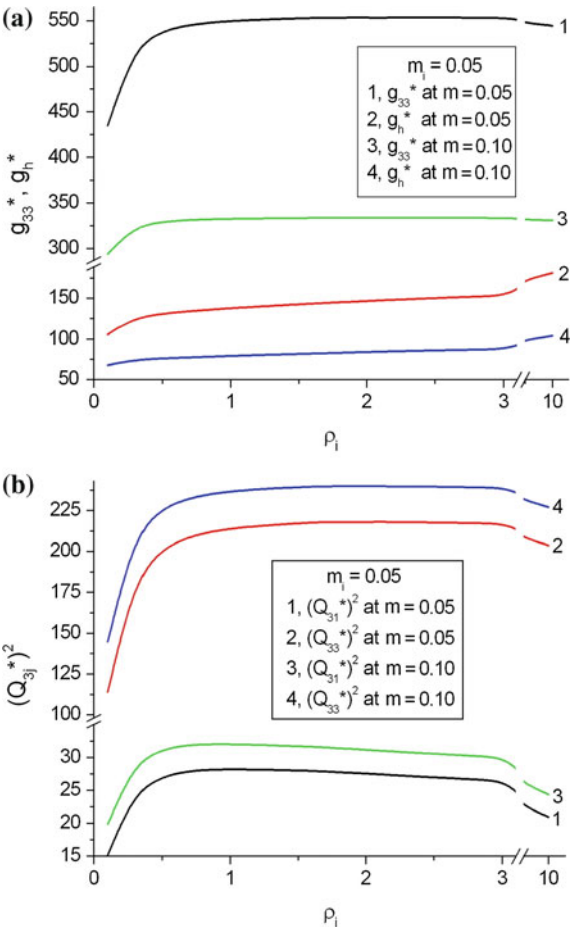

Fig. 13.4 Aspect-ratio (ρ_i) dependence of the piezoelectric coefficient g_{33}^* and hydrostatic piezoelectric coefficient g_h^* (a, in mV · m/N), and squared figures of merit $(Q_{3j}^*)^2$ (b, in 10^{-12} Pa^{-1}) of the 1–0–3 PMN–0.33PT SC/modified $PbTiO_3$ FC/polyurethane composite at volume fractions m_i = const (FC inclusions in the 0–3 matrix) and m = const (SC rods in the composite). At the first stage of averaging, electromechanical properties of the 0–3 matrix were evaluated by EFM (reprinted from Topolov et al. [15], with permission from Elsevier)

changes in m at $m \ll 1$ give rise to considerable changes in the piezoelectric performance and figures of merit of the 1–0–3 composite [4, 15–17].

Third, our results on the performance of the 1–0–3 composites based on SCs are compared to literature data on the 1–3-type piezo-active composites. For instance, work [28] reports a piezoelectric performance of a 1–0–3 FC/FC/polyurethane composite, where the PCR-7 M FC (a PZT-type composition [17]) is the main component. The 1–0–3 PCR-7 M FC/PCR-7 M FC/polyurethane composite is characterized [28] by large piezoelectric coefficients, e.g., $g_{33}^* \approx$ 400 mV · m/N, $g_h^* \approx$ 200 mV · m/N and $d_h^* \approx$ 350 pC/N. The aforementioned parameters are comparable to those given in Tables 13.3 and 13.4. According to data [2], max g_{33}^* related to a 1–3 PMN–0.30PT SC/epoxy composite is 440 mV · m/N (at the volume

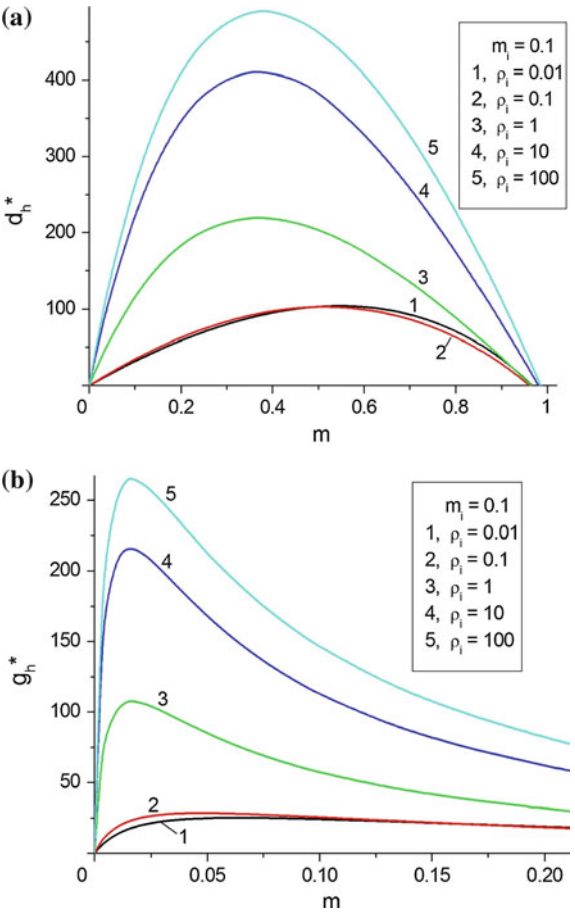

Fig. 13.5 Volume-fraction (m) dependence of hydrostatic piezoelectric coefficients d_h^* (**a** in pC/N) and g_h^* (**b** in mV · m/N) of the 1–0–3 PZN–0.08PT SC/modified $PbTiO_3$ FC/polyurethane composite at m_i = const (reprinted from Topolov et al. [16], with permission from World Scientific)

fraction of SC $m = 0.018$) and is comparable to values of g_{33}^* from Tables 13.3 and 13.4. However, a 1–3 PMN–zPT-based composite from work [29] is characterized by $d_h^* = 111$ pC/N, $g_h^* = 37$ mV · m/N and $(Q_h^*)^2 = 4.12 \cdot 10^{-12}$ Pa^{-1}, and these effective parameters are smaller than those shown in Tables 13.3 and 13.4.

Fourth, data on the squared hydrostatic figure of merit $(Q_h^*)^2 \sim 10^{-12}$ Pa^{-1} (see Fig. 13.2b and Table 13.4) are to be compared to $(Q_h^*)^2$ of the 1–3-type FC-based composites. We note that the $(Q_h^*)^2$ values achieved at small volume fractions of the FC inclusions m_i (see Table 13.4) are approximately equal to $(Q_h^*)^2$ of a 1–3–0 PZT FC/foamed polymer composite [30].

13.4 Conclusions

In the present chapter, we have analyzed the new effects in the piezo-active 1–3-type composites. The first effect is the new orientation effect in the 1–0–3 SC/FC/polymer composite (Fig. 13.1) with two contrasting ferroelectric components (a highly piezo-active SC and highly anisotropic FC) poled on different directions. The second effect is concerned with the active role of the 0–3 matrix and the aspect ratio of its FC inclusions in forming the large hydrostatic parameters of the 1–0–3 SC/FC/polymer composite. Our main research results are concluded as follows.

1. Changes in the rotation angle $\alpha = (\boldsymbol{P}_s^{(1)} \wedge \boldsymbol{P}_r^{(2)})$ (Fig. 13.1) give rise to changes in the elastic and piezoelectric anisotropy of the 0–3 FC/polymer matrix. The $(Pb_{1-x}Ca_x)TiO_3$ FC component plays an important role in the orientation effect due to the large anisotropy of the piezoelectric coefficients $d_{3j}^{(2)}$ in comparison to the anisotropy of $d_{3j}^{(1)}$ of the PMN–0.33PT SC, and due to the high degree of the elastic anisotropy.
2. The orientation effect studied in this 1–0–3 composite leads to a considerable anisotropy of squared figures of merit (5) and a relatively high piezoelectric activity, and such characteristics are of significant interest for the design of high performance composite structures for hydroacoustic, piezoelectric energy harvesting and transducer applications.
3. An important feature of the studied 1–0–3 composite is that elastic properties of its 0–3 matrix considerably depend on the aspect ratio ρ_i of FC inclusions therein and influence the effective electromechanical properties of the 1–0–3 composite in wide aspect-ratio and volume-fraction ranges. This influence becomes important in the presence of two contrasting piezoelectric components. There is no need to pole the 0–3 matrix in a strong electric field, and the high piezoelectric sensitivity is achieved in the case of the non-poled 0–3 matrix with aligned FC inclusions.
4. The electromechanical interaction between the highly piezo-active SC component and the anisotropic 0–3 matrix leads to the creation of high-performance 1–0–3 composite structures. The large values of $g_{33}^* \sim 10^2$ mV · m/N are of significant interest for sensor and receive-type transducer applications, and the large values of $d_h^* \sim 10^2$ pC/N, $g_h^* \sim 10^2$ mV · m/N and $(Q_h^*)^2 \sim 10^{-11}$ Pa^{-1} are of value for hydrophone and related hydroacoustic applications. The large values of the squared figure of merit $(Q_{33}^*)^2 \sim 10^{-10}$ Pa^{-1} and anisotropy $(Q_{33}^*)^2/(Q_{31}^*)^2 \approx 8$–9 are important for piezoelectric energy-harvesting applications.
5. Calculations of effective parameters of the studied 1–0–3 composite were performed using the EFM, FEM and matrix method. Changes in the boundary conditions of the unit cell of the 0–3 matrix with spheroidal FC inclusions, i.e., either Dirichlet (FEM-1) or periodic (FEM-2) boundary conditions, do not give rise to considerable changes in g_h^* and $(Q_h^*)^2$ as predicted by means of the FEM. Results obtained by different ways of averaging the properties at the first and second stages are in agreement.

Acknowledgments The authors thank Prof. Dr. S.-H. Chang (National Kaohsiung Marine University, Taiwan, ROC), Prof. Dr. I.A. Parinov, Prof. Dr. A.E. Panich, Prof. Dr. A.A. Nesterov, and Dr. V.V. Eremkin (Southern Federal University, Russia), and Dr. A.V. Krivoruchko (Don State Technical University, Russia) for their continuing interest in the research problems. The research subject is concerned with the Programme Supporting the Research at the Southern Federal University (Russia). The results on the research work No. 1597 have been represented within the framework of the base part of the state task No. 2014/174 in the scientific activity area at the Southern Federal University (Russia). Prof. Dr. C. R. Bowen acknowledges funding from the European Research Council under the European Union's Seventh Framework Programme (FP/2007-2013)/ ERC Grant Agreement No. 320963 on Novel Energy Materials, Engineering Science and Integrated Systems (NEMESIS).

References

1. K. Ren, Y. Liu, X. Geng, H.F. Hofmann, Q.M. Zhang, IEEE Trans. Ultrason., Ferroelec., a. Freq. Contr. **53**, 631 (2006)
2. F. Wang, C. He, Y. Tang, Mater. Chem. Phys. **105**, 273 (2007)
3. L. Li, S. Zhang, Z. Xu, X. Geng, F. Wen, J. Luo, T.R. Shrout, Appl. Phys. Lett. **104**, 032909 (2014)
4. V.Yu. Topolov, P. Bisegna, C.R. Bowen, *Piezo-active Composites* (Orientation Effects and Anisotropy Factors. Springer, Berlin, Heidelberg, 2014)
5. V.Yu. Topolov, V.R. Bowen, S.V. Glushanin, in *Piezoceramic Materials and Devices*, ed. by I.A. Parinov (Nova Science Publishers, New York, 2010), p. 71
6. R. Zhang, B. Jiang, W. Cao, J. Appl. Phys. **90**, 3471 (2001)
7. R. Zhang, B. Jiang, W. Cao, A. Amin, J. Mater. Sci. Lett. **21**, 1877 (2002)
8. G. Liu, W. Jiang, J. Zhu, W. Cao, Appl. Phys. Lett. **99**, 162901 (2011)
9. J. Yin, B. Jiang, W. Cao, IEEE Trans. Ultrason., Ferroelec., a. Freq. Contr. **47**, 285 (2000)
10. A.V. Krivoruchko, VYu. Topolov, J. Phys. D Appl. Phys. **40**, 7113 (2007)
11. V.Yu. Topolov, A.V. Krivoruchko, J. Appl. Phys. **105**, 074105 (2009)
12. V.Yu. Topolov, A.V. Krivoruchko, Smart Mater. Struct. **18**, 065011 (2009)
13. V.Yu. Topolov, C.R. Bowen, P. Bisegna, S.E. Filippov, in *Nano- and Piezoelectric Technologies, Materials and Devices*, ed. by I.A. Parinov (Nova Science Publishers, New York, 2013), p. 51
14. V.Yu. Topolov, C.R. Bowen, P. Bisegna, A.V. Krivoruchko, Mater. Chem. Phys. **151**, 187 (2015)
15. V.Yu. Topolov, C.R. Bowen, P. Bisegna, Sens. a. Actuat. A Phys. **229**, 94 (2015)
16. V.Yu. Topolov, C.R. Bowen, P. Bisegna, A.E. Panich, Funct. Mater. Lett. **8**, 1550049 (2015)
17. V.Yu. Topolov, C.R. Bowen, *Electromechanical Properties in Composites Based on Ferroelectrics* (Springer, London, 2009)
18. R.E. Newnham, D.P. Skinner, L.E. Cross, Mater. Res. Bull. **13**, 525 (1978)
19. COMSOL, Inc. COMSOLMultiphysics™ User's Guide (version 4.4, 2014), http://www.comsol.com
20. S.V. Glushanin, V.Yu. Topolov, A.V. Krivoruchko, Mater. Chem. Phys. **97**, 357 (2006)
21. S. Ikegami, I. Ueda, T. Nagata, J. Acoust. Soc. Am. **50**, 1060 (1971)
22. F. Levassort, M. Lethiecq, C. Millar, L. Pourcelot, IEEE Trans. Ultrason., Ferroelec., a. Freq. Contr. **45**, 1497 (1998)
23. L.V. Gibiansky, S. Torquato, J. Mech. Phys. Solids **45**, 689 (1997)
24. Y. Xu, *Ferroelectric Materials and Their Applications* (North-Holland, London, 1991)
25. K.H. Yoon, J.H. Yoo, W.S. Kim, E.S. Kim, Ferroelectrics **186**, 169 (1996)
26. S.A. Wilson, G.M. Maistros, R.W. Whatmore, J. Phys. D Appl. Phys. **38**, 175 (2005)

27. C.-W. Nan, L. Liu, D. Guo, L. Li, J. Phys. D Appl. Phys. **33**, 2977 (2000)
28. V.Yu. Topolov, C.R. Bowen, S.E. Filippov, Ferroelectrics **430**, 92 (2012)
29. S. Zhang, F. Li, J. Appl. Phys. **111**, 031301 (2012)
30. E.K. Akdogan, M. Allahverdi, A. Safari, IEEE Trans. Ultrason., Ferroelec., a. Freq. Contr. **52**, 746 (2005)